Accepted Manuscript

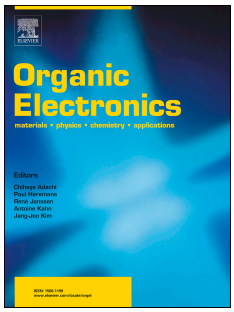

Enhanced photo-stability of inverted organic solar cells via using polyethylenimine in the electron extraction layers

Mozhgan Sadeghianlemraski, Brenda Yasie Lee, Tyler Davidson-Hall, Zoya Leonenko, Hany Aziz

PII: S1566-1199(19)30276-9

DOI: https://doi.org/10.1016/j.orgel.2019.05.048

Reference: ORGELE 5283

To appear in: *Organic Electronics*

Received Date: 3 March 2019

Revised Date: 3 May 2019

Accepted Date: 26 May 2019

Please cite this article as: M. Sadeghianlemraski, B.Y. Lee, T. Davidson-Hall, Z. Leonenko, H. Aziz, Enhanced photo-stability of inverted organic solar cells via using polyethylenimine in the electron extraction layers, *Organic Electronics* (2019), doi: https://doi.org/10.1016/j.orgel.2019.05.048.

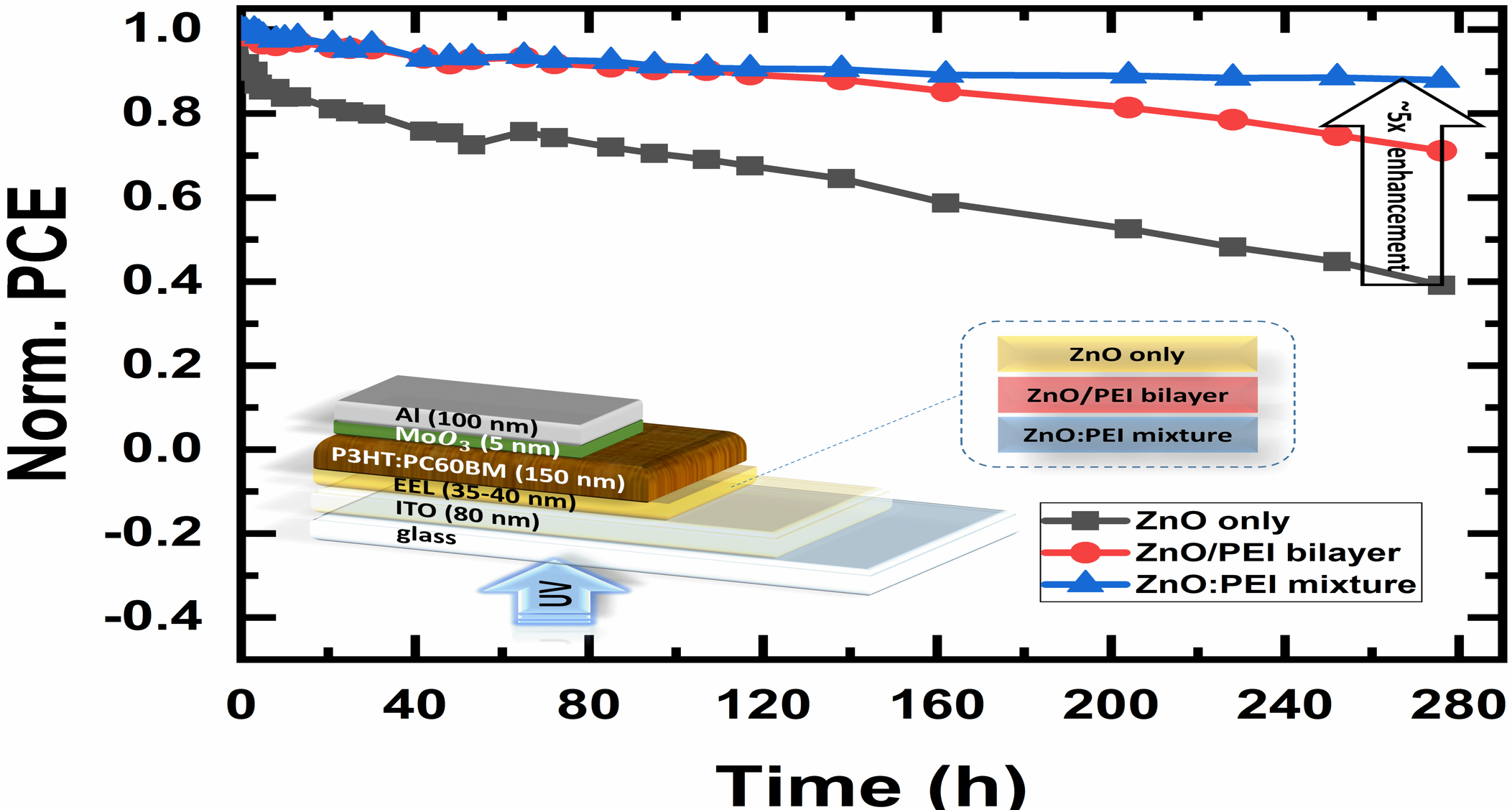
Norm. PCE
1.0
0.8
0.6
0.4
0.2
0.0
-0.2
-0.4
0
40
80
120
160
200
240
280
Time (h)
~5x enhancement
ZnO only
ZnO/PEI bilayer
ZnO:PEI mixture
Al (100 nm)
MoO3 (5 nm)
P3HT:PC60BM (150 nm)
EEL (35-40 nm)
ITO (80 nm)
glass
UV
ZnO only
ZnO/PEI bilayer
ZnO:PEI mixture

Enhanced Photo-stability of Inverted Organic Solar Cells via Using Polyethylenimine in the Electron Extraction Layers

Mozhgan Sadeghianlemraski[1 2], Brenda Yasie Lee[2 3], Tyler Davidson-Hall[1 2,] Zoya Leonenko[2 3], Hany Aziz[1 2]

Abstract

The influence of using Polyethylenimine (PEI) in the electron extraction layers (EELs) on the photo-stability of inverted organic solar cells (OSCs) is investigated. Results show that introducing PEI in the commonly used ZnO EELs, either mixed in the same layer with the ZnO (ZnO:PEI mixture) or in a separate layer in the form of a bilayer EEL configuration (ZnO/PEI), reduces the susceptibility of OSCs to photo-degradation with the mixture giving more significant stability enhancements. In comparison to the widely used ZnO EEL, the use of ZnO:PEI mixture is found to lead to ~ 5x higher PCE stability under continuous UV irradiation, the latter being the main factor behind the limited stability of the cells under sunlight, primarily due to a more stable V_{oc} and FF. Tests on electron only devices show that the higher photo-stability is mainly due to the role of the ZnO:PEI mixture in minimizing light-induced deterioration in electron collection efficiency at OSCs electron collection contacts under sunlight. Kelvin probe force microscopy (KPFM) measurements show that the use of ZnO:PEI helps maintain a more stable surface potential at the electron collection contact, hence the more stable V_{oc} and FF. X-ray photoelectron spectroscopy (XPS) measurements reveal that the stability enhancement is likely associated with chemical interactions between PEI and ITO at the ITO/ZnO:PEI interface that produce a more electronically and energetically stable contact that is less susceptible to changes in surface potential or work function by UV illumination. Using PEI in the form of a neat layer next to the ITO in a bilayer EEL (PEI/ZnO) is found to provide a similar significant enhancement in photo-stability, further ascertaining the above conclusions.

[1] Department of Electrical and Computer Engineering, University of Waterloo, 200 University Avenue West, Waterloo, ON N2L 3G1, Canada.

[2] Waterloo Institute of Nanotechnology, University of Waterloo, 200 University Avenue West, Waterloo, ON N2L 3G1, Canada.

[3] Department of Physics & Astronomy, University of Waterloo, 200 University Avenue West, Waterloo, ON N2L 3G1, Canada.

The findings not only reveal the potential of utilizing PEI in the EEL, but also shed light on some of the root causes of the limited photo-stability of OSCs and approaches to mitigate their effect.

Keywords: electron extraction layer, polyethylenimine (PEI), organic solar cells, photo-stability, photo-induced deterioration, surface potential.

1. Introduction

Organic solar cells (OSCs) are attracting tremendous interest due to their mechanical flexibility, versatile form factors and compatibility with low-cost mass production fabrication technology [1-5]. Two main factors however continue to limit their commercialization; their relatively limited efficiency and stability. While the limited efficiency issue of OSCs has been the focus of a vast body of work, addressing the stability issue has received much less attention in comparison. In polymer OSCs, degradation proceeds in the form of a gradual decrease in power conversion efficiency (PCE) with time. This degradation arises from various aging phenomena that - in general - are induced by either oxygen or moisture from the ambient or by solar irradiation; the latter mostly due to the ultraviolet (UV) components of the solar spectrum [6−8]. Advancements in developing encapsulation technologies make it now possible to effectively control ambient-induced degradation. With that, solar irradiation-induced degradation (usually referred to as photo-degradation), becomes one of the remaining challenges that need to be overcome for commercialization. [7–9].

To attain high efficiency and long-term photo-stability, an appropriate selection of electron extraction layer (EEL) is critical [10-13]. We have previously demonstrated that aside from the enhancement of photovoltaic (PV) characteristics, certain EELs can also significantly reduce the susceptibility of metal contact interfaces to photo-degradation, thus lead to improved OSC photo-stability [11-13]. According to the electron and hole collection directions, OSC architectures can generally be divided into conventional (i.e. upright) and inverted geometries. The use of a high work function (WF)

top metal in case of inverted OSCs gives them an advantage in terms of ambient stability [14]. In inverted OSCs, ZnO is the most commonly used EEL material due to its high transparency, relatively high electron mobility, solution processability and environmental stability [15-19]. Despite its advantages, ZnO has some shortcomings including the presence of vacancies that causes some charge loss [20] and a relatively high WF that leads to a high barrier for charge collection from organic acceptor materials [21,22]. In this regard, it was recently shown that using polymeric surface modifiers, such as polyethylenimine (PEI) [23-25] and ethoxylated polyethylenimine (PEIE) [6, 26, 27], with ZnO can adjust its WF as a result of the formation of an interfacial dipole layer at the ZnO/PEI interface and lead to improvements in device performance. However, the low conductivity of these polymers poses challenges, inspiring the idea of using a ZnO:PEI mixture composite as an alternative approach [28-30]. Jia et al. showed that using neat PEI on ITO as an EEL can give a similar performance to ZnO as long as it is kept to a very thin layer, whereas using ZnO:PEI mixture allows using thicker layers and enhances device performance [29]. Using ZnO:PEI composite cathode interlayer, Liu et al. demonstrated OSCs with a PCE of 9.90%, an open circuit voltage (V_{oc}) of 0.760 V, a short-circuit current density (Jsc) of 17.80 mA/cm2, and a fill factor (FF) of 73.15% via Poly[[4,8-bis[(2-ethylhexyl)oxy]benzo[1,2-b:4,5-b']dithiophene-2,6-diyl][3-fluoro-2-[(2 ethylhexyl)carbonyl]thieno[3,4-b]thiophenediyl]] (PTB7): [6,6]-Phenyl-C71-butyric acid methyl ester (PC71BM) as an active layer. They also showed that mixing ZnO with a small amount of PEI modifies its WF without appreciably affecting conductivity, optical transmission or film morphology [30]. Venkatesan et al [6] showed that introducing a layer of PEIE on ZnO EEL or AZO (Aluminum-doped ZnO) cathode of OSCs can increase their ambient stability; an effect that was attributed to suppressing surface oxidation of the metal oxide layers. Shafket et al. [31] recently showed that mixing ZnO with PEIE, when used along with an additional layer of the latter, can improve the light-soaking behavior of OSCs under UV-free irradiation.

While the use of PEI in EELs in OSCs is starting to gain momentum in the field, its influence on the photo-stability of the cells has not yet been studied to the best of our knowledge. Knowing from our previous work [10-13] that EELs can significantly influence OSC photo-stability, it becomes important to

investigate that behavior with this new EEL material system. With recent findings by Tournebize et al. of UV-induced shunt formation at the ZnO/active layer interface and the potential benefits of using buffer interfacial layers as a possible way to help eliminate that behavior [32], investigating the effect of modifying that interface on OSC photostability becomes even more compelling. Therefore, in this work, we systematically investigate and compare the behavior of inverted OSCs with ZnO, ZnO/PEI (bilayer) and ZnO:PEI (mixture) EELs, utilizing for that purpose the archetypal Poly(3-hexylthiophene) (P3HT): [6,6]-Phenyl C61 butyric acid methyl ester (PC60BM) OSC donor:acceptor system. Results reveal that using ZnO:PEI EELs leads to significant improvements in OSC photo-stability, resulting in ~5x higher photo-stability (around 12% decrease of its initial PCE after 276h of UV irradiation vs 60% in case of ZnO EEL). The stability enhancement is attributed primarily to a much more stable open circuit voltage (V_{oc}), the latter being the parameter that typically degrades the fastest in inverted OSCs under UV [32]. Findings from electron-only devices as well as atomic force microscopy (AFM), Kelvin probe force microscopy (KPFM) and X-ray photoelectron spectroscopy (XPS) measurements reveal that the ITO/EEL interface plays a more influential role in the photo-degradation behavior of OSCs relative to the EEL/bulk hetero-junction (BHJ) interface, contrary to what was believed before.

2. Experimental

2.1. Material Preparation and Device Fabrication:

In this work, BHJ OSCs using the archetypical P3HT:PCBM donor:acceptor system in the widely used inverted architecture of the structure: ITO/EEL/P3HT:$PC_{60}BM$/MoO_3/Al, utilizing ZnO, ZnO/PEI bilayer (40 nm) or ZnO:PEI mixture as EEL were used. The OSCs were fabricated on 80 nm thick ITO patterned glass substrates (Kintec) with a sheet resistance of 15 Ω sq^{-1}. In these devices, the ITO, P3HT:PC60BM, MoO_3 and Al served as cathode, active layer, hole extraction layer (HEL) and anode respectively.

ZnO synthesis was done following the standard approach as reported previously [33]. PEI (Sigma-Aldrich) was diluted in 1-propanol to reach a 0.5 mg/ml solution and then mixed with 32 mg/ml ZnO solution to prepare ZnO:PEI mixtures of various PEI concentrations (0.01, 0.02, 0.03 or 0.04 %wt PEI).

To prepare the active layer solution, poly (3-hexylthiophene) (P3HT) from Sigma Aldrich and [6,6]-Phenyl C61 butyric acid methyl ester (PC60BM) from 1-material company were diluted in dichlorobenzene (Sigma Aldrich) in a 1:1 ratio to obtain a 45 mg/mL concentration and then stirred at 100 ° C and 650 rpm overnight.

For OSC fabrication, the substrates were first cleaned via sequential ultrasonic treatments using Micro 90, deionized water, acetone and isopropanol solutions and then treated with O_2 plasma for 5 min. Samples were then transferred to a nitrogen-filled glovebox. For coating the electron extraction layers. ZnO was spun coated at 1000 rpm for 60s with annealing condition of 150 °C for 30 min, PEI and ZnO:PEI were spun coated at 5000 rpm for 60s before annealing at 120 °C for 20 min and 150 °C for 30 min, respectively. The P3HT:PC60BM BHJ active layer was then deposited on the ITO/ZnO, ZnO/PEI (bilayer) or ITO/ ZnO:PEI (mixture) EEL. The BHJ layer was coated at 1000 rpm for 80 s and annealed at 150°C for 30 min on a hot plate, resulting a thickness of ~150 nm. After that, samples were transferred to an Angstrom Engineering EvoVac thermal evaporation chamber with a base pressure of 5 × 10−6 Torr to deposit 5 nm of MoO_3 (American Elements), and 100 nm of aluminum anode (Angstrom Engineering). 14 OSCs were fabricated on each substrate. The surface area of each OSC was 0.04 cm^2 and was determined by the intersection area of the anode (Al) and cathode (ITO) electrodes. In order to have a more accurate comparison between the different EELs and reduce other confounding factors (small variations in MoO_3 or Al deposition and/or vacuum pump-down cycles), each substrate was first cut into 4 equal pieces and a different EEL (ZnO, ZnO/PEI (bilayer) or ZnO:PEI (mixture)) was spun coated on each piece, followed by the active layer. The 4 pieces were then taped together and mounted in the vacuum system for the deposition of the MoO_3 and Al layers. In the case of OSCs with Poly [N-9'-heptadecanyl-2,7-carbazole-alt-5,5-(4',7'-di-2-thienyl-2',1',3'-benzothiadiazole)] (PCDTBT):PC70BM,

the active layer solution, PCDTBT:PC70BM (Sigma Aldrich) is dissolved in dichlorobenzene with a ratio of 1:4, and then stirred at 100 ° C and 650 rpm overnight to obtain a 25 mg/mL concentration. In this case, the layer was spun coated at 700 rpm for 1min, and annealed at 100 °C to achieve a 80 nm film.

Electron only devices (EODs) were fabricated following the same procedure used for the OSCs. 1,3,5-tris(N-phenyl-benzimidazol-2-yl)-benzene (TPBi) purchased from Electronic Materials Index Co, and lithium fluoride (LiF) from Sigma Aldrich were deposited by evaporation.

2.2. Material and Device Characterization:

Current density–voltage (J–V) characteristics were measured under 1-sun AM1.5G illumination from an ABET Sun 3000 Class AAA solar simulator using a Keithley 2400 source meter. Photo-stability tests are performed using illumination from a UV source at a wavelength of 365 nm and an illumination power density of 0.8 W/cm^2 with the the samples being kept in a N_2 environment and fan-cooled during the test to keep them at room temperature.

Atomic force microscopy and Kelvin probe force microscopy to obtain simultaneous topographical and contact potential difference (CPD) images in air was done using an AIST-NT™ SmartSPM 1000 atomic force microscope. A single MikroMasch® HQ:NSC14 Au coated conductive probes were used to take these images, with a tip radius of approximately 35 nm, resonance frequency of 160 kHz, a force constant of 5 N/m, and a length of 125 µm ± 5 µm. At least two 5 x 5 µm images were taken for each of the two samples made in each trial. From these images, at least 100 measurements were taken from different areas to determine the average CPD and height values. Roughness measurements of the AFM images were also taken. XPS measurements were performed by Thermo-VG Scientific ESCALab 250 Microprobe equipped with a monochromatic Al Kalpha X-ray source (1486.6 eV).

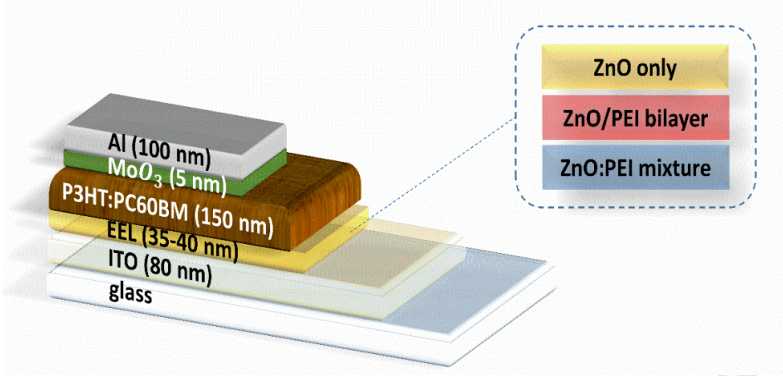

Figure 1. *A schematic depiction of the structure of the OSCs used in this work.*

3. Results and Discussion

Three groups of OSCs of the structure: ITO/EEL/P3HT:$PC_{60}BM$/MoO_3/Al, each consisting of 8 identical cells, utilizing ZnO, ZnO/PEI bilayer or ZnO:PEI mixture as EEL were fabricated. The EEL thickness was approximately 35-40 nm in all cases. This included the thickness of the PEI layer (~ 5-7 nm) in case of the ZnO/PEI EEL. Figure 1 depicts the device structures. All devices were fabricated and tested under the same conditions. The PV parameters of these cells under 1 sun 1.5 AM radiation are provided in Table 1, where all numbers represent average values from the 8 cells in the group except for the last row which presents the maximum PCE value in each group. The J-V characteristics of the cells with the highest PCE in each group are provided in (Figure S1.) We should point out that the specific ZnO:PEI mixing ratio (1:0.04 by weight) was selected based on preliminary work that showed that it gave better photovoltaic performance relative to other ratios (data from that work is provided in Table S1).

As can be seen from the data in Table 1, devices with ZnO EEL, which are used here as reference devices, demonstrate an initial PCE of about 2.4%; on par with other reports for this device structure [32]. Generally, the PV parameters of devices from the three groups are comparable, with the ZnO:PEI EEL devices having somewhat higher PCE and J_{sc}, exhibiting average and maximum PCE of 2.56% and 2.75%, respectively versus 2.38% and 2.46% in case of the ZnO reference devices, and a J_{sc} of 6.43 mA/cm^2 versus 6.25 mA/cm^2 in case of the reference devices. The small increase in J_{sc} on using ZnO:PEI instead of ZnO as EEL is in good agreement with previous reports [29]. We note that the J_{sc} in

case of the ZnO/PEI devices was generally somewhat lower than in the ZnO case in our devices and was in line with the work by Venkatesan et al [6].

Table 1. *PV parameters of OSCs with the ZnO, ZnO/PEI (bilayer) and ZnO:PEI (mixture) EELs.*

EEL / ***Parameters***	***ZnO***	***ZnO/PEI bilayer***	***ZnO:PEI mixture***
$J_{sc}(mA/cm^2)$	6.25 ± 0.55	5.33 ± 0.23	6.43 ± 0.31
$V_{oc}\ (mV)$	668.58 ± 14.4	666.98 ± 13.4	672.45 ± 4.6
FF [%]	57.11 ± 3.17	59.99 ± 1.47	59.25 ± 1.23
$R_{shunt}\ (Ohm.\ cm^2)$	23367 ± 4110	27842 ± 7136	22149 ± 2837
$R_{series}\ (Ohm.\ cm^2)$	13.12 ± 5.03	8.61 ± 2.22	9.16 ± 1.11
$Ave - PCE$ [%]	2.38 ± 0.07	2.13 ± 0.11	2.56 ± 0.14
$max - PCE$ [%]	2.46	2.38	2.75

In order to investigate and compare between the photo-stability performance of the OSCs, the devices were exposed to continuous illumination from a 365 nm UV source at an illumination power density of 0.8 W/cm^2. The wavelength is representative of the long wavelength portion of the UV_A range of the solar spectrum capable of reaching the earth surface which is known to be a primary cause of photo-degradation in OSCs [17, 32, 34, 35]. The J-V characteristics (again under 1 sun, AM 1.5) of the OSCs were collected at various times during the UV exposure (with the UV illumination temporarily blocked during the measurements to prevent contributions from the UV illumination to carrier photo-generation). Figure 2 shows the obtained PCE, V_{oc}, FF and Jsc at those times, normalized to their initial (i.e. time zero) values. As can be seen from the figure, prolonged exposure to UV causes a deterioration in the PV parameters of all devices as expected, but the degradation was slower in case of the devices containing PEI in their EELs. Remarkably, the ZnO:PEI OSC exhibited significantly higher stability, showing only about 12% decrease in PCE after 276h UV irradiation, ~ 5x smaller than that observed in

case of the ZnO OSC. The largest difference is observed in V_{oc} and FF, with the earlier showing a decrease of 1.26%, 11.9% and 29.5% in the devices with the ZnO:PEI, ZnO/PEI and ZnO EELs, respectively, after 276 hours of UV exposure. It should be noted that this large degradation in V_{oc} in case of the control device is consistent with literature [6, 32, 34, 35]. Besides, we note that the V_{oc} photo-stability of OSCs with ZnO/PEI EEL is somewhat higher than the ZnO-based devices while lower than the cells with ZnO:PEI EEL. In contrast, the J_{sc} degradation trends were comparable in all devices, with the ZnO OSC showing only slightly faster degradation than the other two devices. The comparable loss in J_{sc} indicates that, unlike V_{oc} and FF, its origins are independent of the EEL, and suggests it may be associated with changes in the active layer bulk, perhaps due to $PC_{60}BM$ dimerization [6, 17, 32, 34, 36].

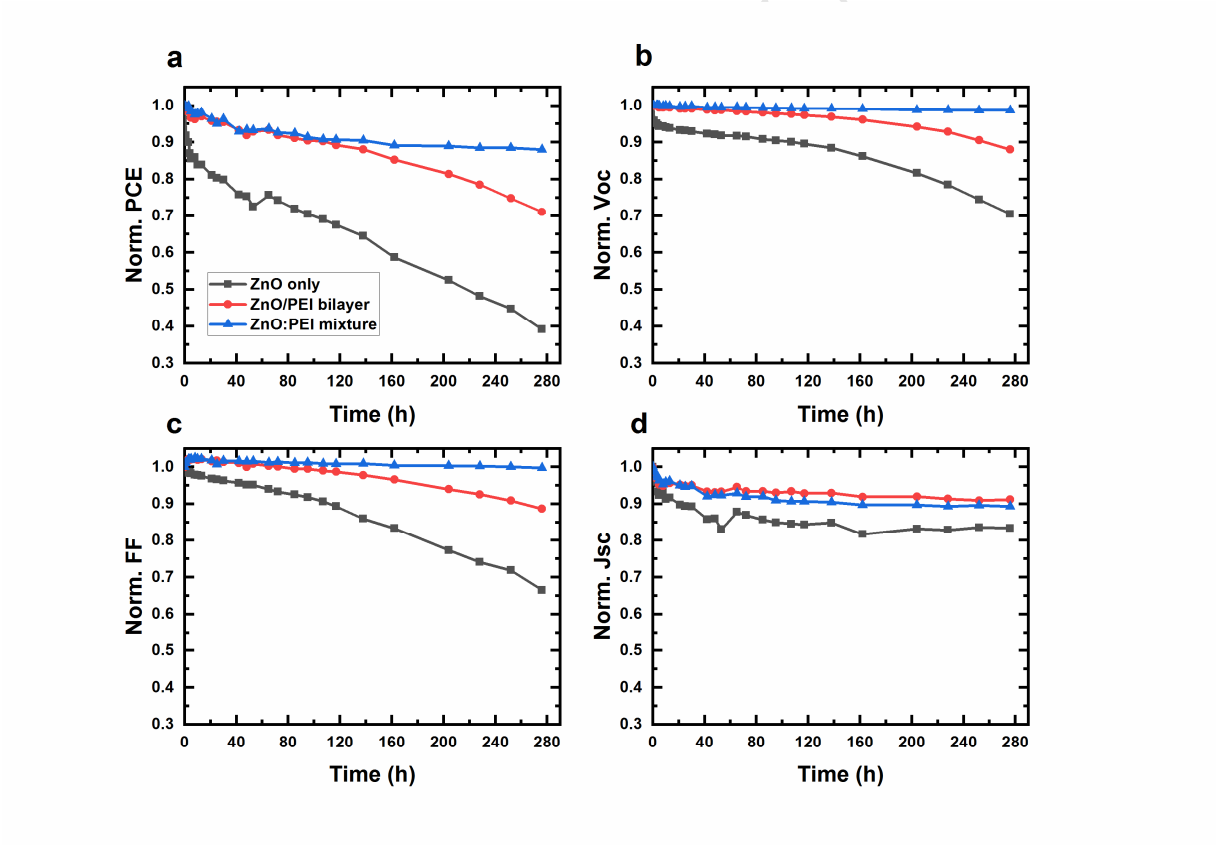

Figure 2. *Normalized PCE (a), V_{oc} (b), FF (c), and J_{sc} (d) versus time under continuous UV illumination of OSCs with the ZnO, ZnO/PEI and ZnO:PEI EELs.*

Table 2. *% change in PV parameters of OSCs with the different EELs after 276 hours of UV irradiation and of a control set of identical OSCs that was kept in the dark (i.e. no UV) for the same period of time.*

Parameters	**%ΔJsc**		**%ΔVoc**		**%ΔFF**		**%ΔPCE**	
EELs	**Control**	**UV**	**Control**	**UV**	**Control**	**UV**	**Control**	**UV**
ZnO	-6.54	-16.6	-1.43	-29.5	+0.83	-33.5	-6.71	-60.87
ZnO/PEI bilayer	-4.33	-8.83	-1.08	-11.9	+0.33	-11.35	-5.06	-28.9
Mixed ZnO:PEI	-6	-10.69	-0.016	-1.26	+0.45	-0.25	-1.74	-12

In order to determine if the observed changes in the PV characteristics of the OSCs were indeed caused by the UV illumination, we similarly tested the J-V characteristics of an identical set of devices that was kept in the dark over the same period of time to be used as a control set for comparison. Table 2 compares the changes in the PV parameters of the UV-illuminated and the control devices over the same period of time (276 hours). Clearly, the control devices exhibit much smaller changes in their PV parameters in comparison, verifying that the degradation observed in case of the UV-illuminated devices was indeed mostly caused by the UV exposure. Considering that the only difference between the three sets of devices is their EELs, the significant differences in their photo-stability behavior must be associated with the EELs, and more specifically their (i.e. the EEL's) role in influencing the stability of the V_{oc} and FF over time, and, as a result, PCE.

In order to identify the role of the ZnO/PEI and ZnO:PEI EELs in increasing the photo-stability of the OSCs and to investigate whether it is associated with improving the stability of the electron collection contact and reducing its susceptibility to photo-induced degradation [12-14], we test the EELs in EODs. First, we incorporate the EELs in EODs of the structure: ITO/ EEL/ 2,2′,2"-(1,3,5-Benzinetriyl)-tris(1-phenyl-1-H-benzimidazole) (TPBi)/LiF/Al. The device structure is depicted in the inset of figure 3(a). In these devices, TPBi, an electron transport material, is used because of its relatively

high electron mobility and low optical absorption at 365 nm [37] which makes it not susceptible to photo-degradation by the UV illumination. As such, any changes in the electrical characteristics of the devices due to UV illumination will not be due to changes in the TPBi layer. Under forward bias, defined as holding the Al electrode at a more negative potential relative to the ITO contact, electrons are efficiently injected from the LiF/Al contact and transported into the TPBi and then into the EELs before they eventually get collected at the ITO contact. Thus, in these devices, the direction of electron transport in the EELs and their collection at the ITO/EEL contacts resembles that of the photo-generated electrons in case of the OSCs. In contrast, hole injection from the ITO contacts under the same bias direction is obstructed by the large energy offset between the ITO work function and the valence band of the ZnO. As such, the flow of current occurs almost exclusively via electrons. Figure 3(a) shows J-V characteristics of these EODs with the different EELs, collected in the dark. As can be seen, the use of ZnO:PEI EEL leads to a higher current relative to the other devices at any given driving voltage pointing to its higher conductivity and/or more efficient electron collection at the two EEL interfaces. As the EODs with the ZnO and ZnO/PEI EELs have different EEL/TPBi interfaces (no PEI in the first vs. PEI in the second), their similar J-V characteristics suggest that the EEL/TPBi interface does not strongly influence or limit electron collection in these devices, indicating that the higher current in case of the ZnO:PEI is not due to easier electron collection at the ZnO:PEI/TPBi contact and is therefore due to the higher bulk conductivity of the ZnO:PEI and/or more efficient electron collection at the ITO/ZnO:PEI contact.

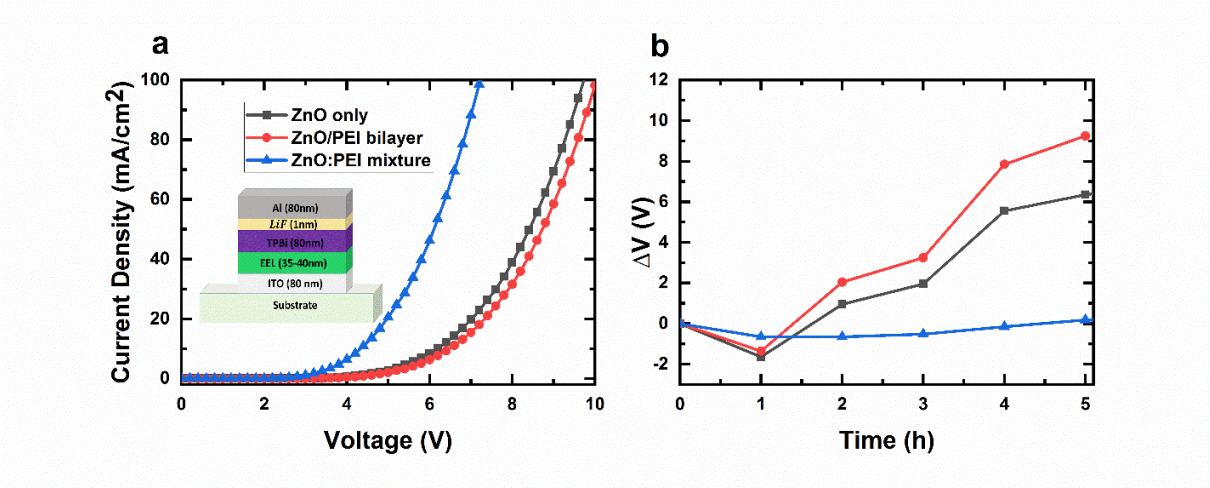

Figure 3. *a) JV characteristics collected in the dark for EODs with ZnO, ZnO/PEI or ZnO:PEI contacts. Insets: the structure of EODs used in this work. b) Net change in driving voltage (ΔV), defined as voltage needed to maintain a current density of 20 mA/cm^2 at any time t minus the initial voltage at the same current density, under 5h UV illumination for the 3 contacts of interest.*

One set of EODs was then exposed to continuous UV illumination (same conditions as above) and their J-V characteristics were measured (in the dark) at certain time intervals. Changes in their forward bias driving voltage, defined as the voltage needed to maintain a constant current density of 20 mA/cm^2, and presented in the form of the net change in voltage $\Delta V =$ the voltage at any time t minus the initial voltage, are provided in Figure 3(b). Clearly, the illumination causes a faster rise in the driving voltage over time in case of the EODs with the ZnO and ZnO/PEI EELs indicating that electron transport and collection becomes increasingly less efficient. In contrast, the driving voltage trend of the EOD with the ZnO:PEI EEL remained remarkably much more stable, pointing to the role of this EEL in reducing photo-induced deterioration in electron transport and collection, and maintaining efficient electron collection over time. It is also clear that although the EODs with the ZnO and ZnO/PEI EELs have different EEL/TPBi interfaces, they both exhibit low stability. We also test a set of EODs of the structure ITO/ EEL/P3HT:PC60BM/TPBi/ LiF/Al (depicted in the inset of Figure S2 (a)) to verify if similar trends are observed when the EEL is in contact with the BHJ (instead of TPBi) as is the case in the OSCs. The results from those devices are presented in Figure S2 (b), confirming that this indeed is the case, where

again the EOD with the ZnO:PEI exhibits the most stable voltage trend. It follows from these results that the much higher photo-stability of the ZnO:PEI EEL must be related to factors associated with the EEL bulk and/or the ITO/EEL interface (which, in this case, can be expected to be altered due to the presence of PEI in the mixture) in influencing the photo-stability behavior of OSCs. Although higher photo-stability of the OSCs with ZnO/PEI EEL compared to the ZnO-based cells suggests that having PEI at the BHJ interface may have some photo-stability benefits for the BHJ as was also reported recently [32], the fact that the EODs with the ZnO and ZnO/PEI EELs generally have similar stability trends shows that the EEL/BHJ interface plays a smaller role in comparison in influencing the photostability behavior of the OSCs. It should be pointed out that this is different from the short-term "light-soaking" behavior observed in OSCs with metal-oxide EELs, especially those processed in air, which, in contrast, is more strongly influenced by the EEL/BHJ interface [34, 38].

Finding out that the ZnO:PEI EEL leads to a significant enhancement in OSC photo-stability and that the effect is most likely due to maintaining a more stable electron collection efficiency across the EEL and/or ITO/EEL contact, it becomes important to investigate the root causes of this behavior. We, therefore, use AFM and KPFM to respectively study the morphological and electrical surface potential characteristics of the ZnO, ZnO/PEI and ZnO:PEI as well as of the bare ITO, and to probe any changes in those characteristics under UV illumination.

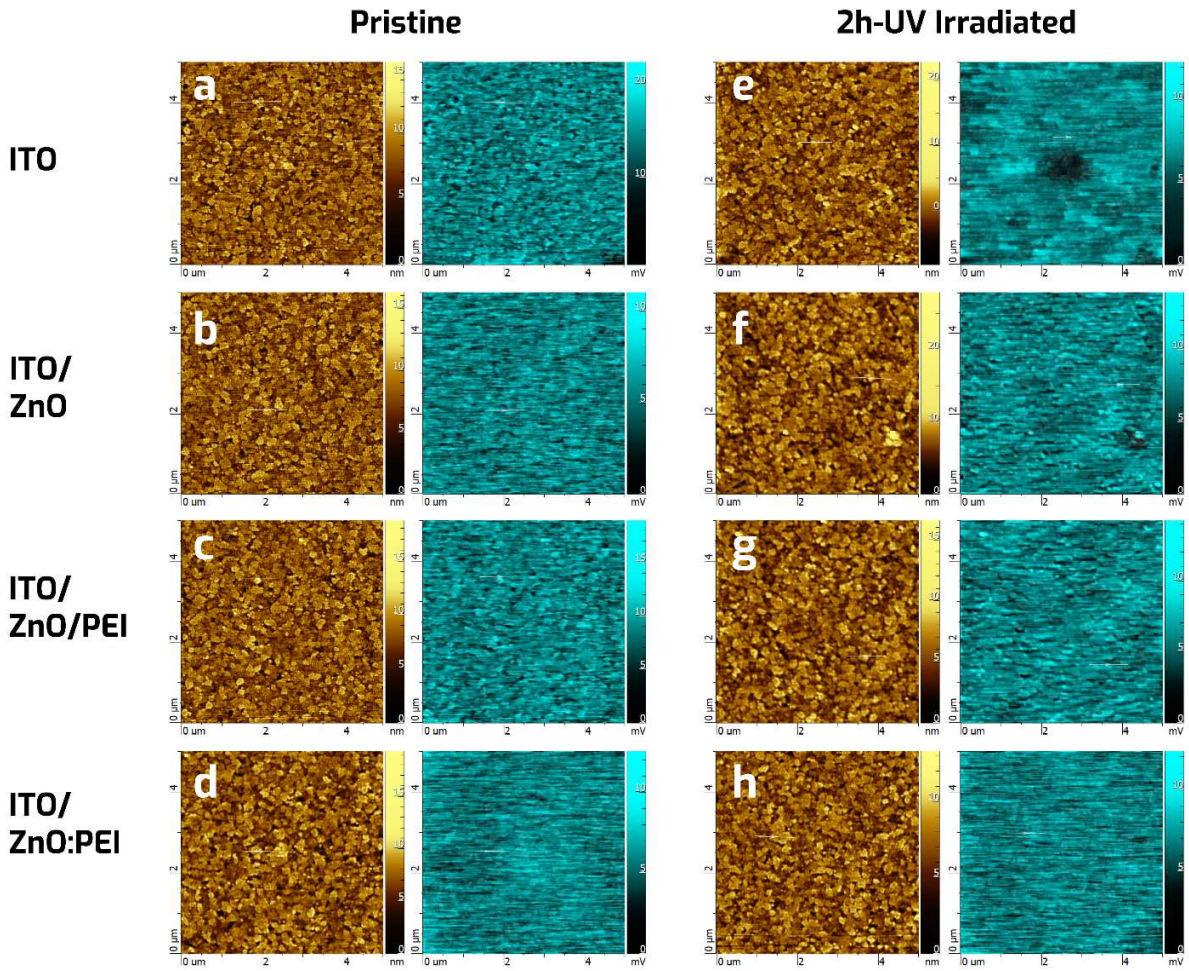

Figure 4. *AFM (golden) and KPFM (blue) images of ITO Control, ZnO, ZnO/PEI and ZnO:PEI films; before (a, b, and c, d respectively) and after 2 hours UV exposure (e, f, g, and h).*

AFM images (golden) and KPFM images (blue) collected from ITO, ITO/ZnO, ITO/ZnO/PEI and ITO/ZnO:PEI films before (pristine) and after UV exposure for 2 hours are provided in Figure 4. The images were collected simultaneously form the same sample area in order to allow comparing their surface topography and electrical surface potential. To obtain the KPFM images, the surface of the sample is scanned with a probe tip that measures the potential difference, CPD, between the sample surface and the tip. This potential difference will generally depend on the work function of the surface and tip materials as well as on the electrical surface potential of material surfaces. Although the absolute

value of the measured CPD depends on the specific experimental setup, imaging the sample surface with the same probe can reveal differences in electrical surface potential.

Looking at the AFM images, a comparison of all the pristine films (Figure 4(a)-(d)) shows that they all have similar surface topography with the ITO/ZnO:PEI film having a slightly smoother surface relative to ITO/ZnO, ITO/ZnO/PEI and the ITO control, with a root-mean-square roughness (R_{rms}) of 1.34 nm ± 0.01 nm versus 1.41 nm ± 0.08 nm, 1.42 nm ± 0.10 nm and 1.40 nm ± 0.09 nm in the other three films, respectively. After UV exposure (Figure 4(e)-(h)), the R_{rms} is found to change slightly for each film, with the ITO/ZnO film being affected the most (by about 0.4 nm instead of 0.1 nm in the other films). While the increase in roughness might suggest that ZnO is susceptible to UV-induced aggregation, a phenomenon observed in other materials [39, 40], the morphological differences among the samples were too small to be expected to play a major role in the different photo-stability behavior of the EELs.

Figure 5 gives the average CPD values obtained from KPFM scans of the sample surfaces at various times with the samples initially being kept in the dark (for 2 hours), followed by UV illumination (for 2 hours), and then again being kept in the dark (for 28 hours). The averages are obtained from measuring CPD at 100 different points on the surface of each sample at the given times. As can be seen from the figure, CPD does not change appreciably in all samples while in the dark. Illumination, however, leads to significant changes in CPD in case of ITO, ITO/ZnO and ITO/ZnO/PEI samples, pointing to UV-induced changes in surface potential. In contrast, the changes in CPD due to the UV exposure were much smaller in case of the ITO/ZnO:PEI sample. It is worth pointing out that the photo-induced changes in surface potential do not show any significant changes upon leaving the samples in the dark for 28 hours following the illumination. This shows that the photo-induced degradation is not reversible in the dark, at least when no external stimulus such as a reverse bias is applied [41, 42]. As changes in electrical surface potential of a sample mirror changes in its electrical properties including work function [43], the results suggest that the exposure to UV brings about more significant changes in work function in case of the ZnO and ZnO/PEI EELs than in case of the ZnO:PEI EEL. It is for example known that although UV

illumination can initially improve the performance of OSCs, prolonged illumination can induce the formation of chemical defects and the introduction of interstitial oxygen in ZnO that lead to an increase in its work function and reduce its n-type characteristics in the longer term [34, 41,44]. The fact that a similar change in electrical surface potential is observed in case of the ITO/ZnO/PEI, where the presence of the PEI would expectedly interfere with reactions between oxygen and ZnO surface, suggests that additional factors, including ones that may not necessarily be at the stack surface, could however be involved. It is, for example, possible that the changes arise from a shift in ITO work function which is also known to occur under illumination [46-47]; such an effect is also evident from the changes in CPD of the bare ITO samples measured here. A change in ITO work function could lead to a change in the surface potential of subsequent layers due to a vacuum level shift at the ITO/EEL interface. In this context, the use of ZnO:PEI instead of neat ZnO may perhaps alter this behavior, and thereby stabilize ITO work function. Regardless of the specific underlying factors, the results clearly show that the surface potential of the ITO/ZnO:PEI remains relatively unchanged under UV illumination, an effect that is clearly different from that observed with the other EELs or the bare ITO. This may explain the enhanced V_{oc} photo-stability of OSCs utilizing this EEL [6].

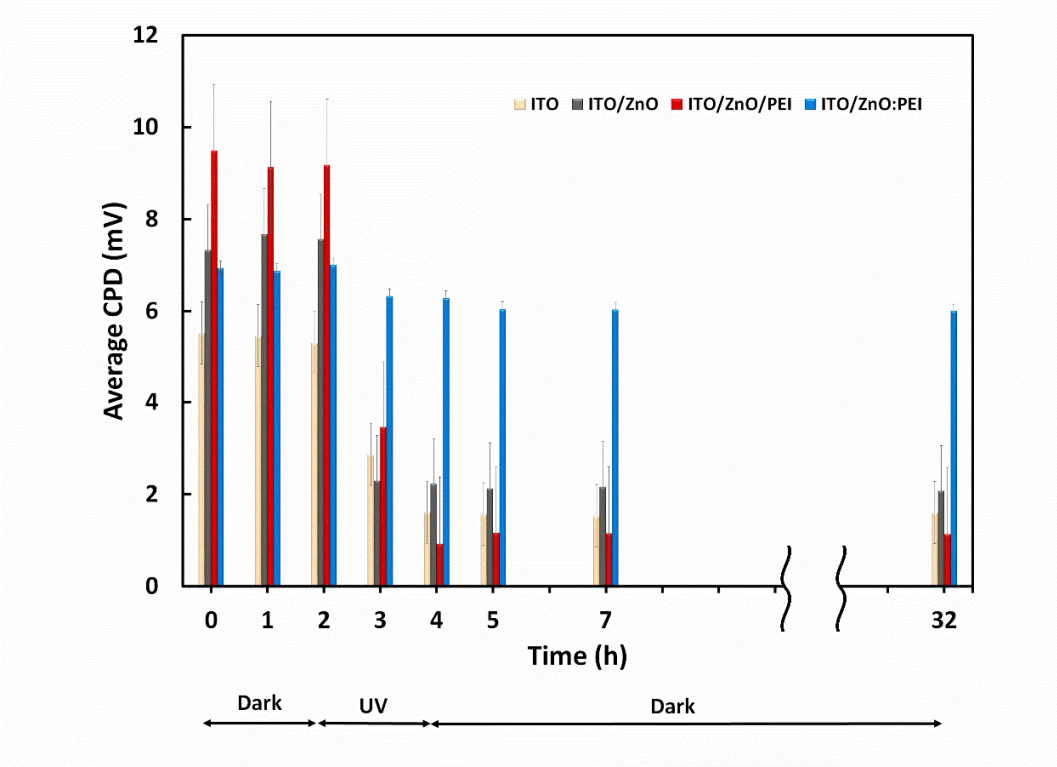

Figure 5. *Average CPD versus time for the ITO, ITO/ZnO, ITO/ZnO/PEI and ITO/ZnO:PEI samples. The samples were kept in the dark during the first 2 hours, exposed to UV illumination during the next 2 hours and then kept in the dark again during the last 28 hours. The height of each column represents the average value of 100 points on the sample surface.*

In order to investigate the origins of the different behavior of the CPD in the ITO/ZnO:PEI *vs* the other samples, we use XPS measurements to study and test for any changes in the surface chemistry of the UV-exposed versus pristine ITO, ITO/ZnO:PEI and ITO/ZnO films. The XPS scans of the binding energy of the C 1s and O 1s peaks for ITO sample and C 1s electrons for ITO/ZnO and ITO/ZnO:PEI samples are presented in supporting information (Figure S3). Figure 6 shows O 1s and Zn 2p peaks for the ITO/ZnO:PEI and ITO/ZnO samples. In order to probe the effect of UV illumination on the ITO/EEL in case of the ITO/ZnO:PEI and ITO/ZnO samples, we also collect XPS scans after sputtering the sample for 300s using Ar+ in order to remove the EEL. CASAXPS software was used for analyzing the XPS spectra including quantification and band deconvolution.

First, looking at results from the bare ITO samples, the surface C 1s spectrum (Figure S3.a) can be resolved into 4 bands, with peaks at 285.5, 287.2, 289 and 291.2 eV for the pristine ITO film, which

can be assigned to various C-C and C-O bonds. The presence of some of these bands may be attributed to contamination from the tape used for mounting the samples. The UV exposure caused the 291.2 eV band to disappear and altered the relative intensities of the other three bands. The O 1s spectrum of the ITO surface (Figure S3.b) showed 2 distinct peaks and can be de-convoluted to 3 bands, with maxima at 530.5, 531.9 and 534.9 eV in case of the pristine ITO, with one of them, the 534.9 eV band, again absent in case of the UV-exposed ITO. This band can be attributed to carbonyl oxygen [32], perhaps associated with reactions between chemisorbed O (from the ambient or released from the ITO surface) and C (from the sample environment) on the ITO surface. UV illumination causes the photo-oxidation or these organic contaminants and/or the dissociation of these O-C bonds, leading to their disappearance from the spectrum of the UV exposed samples. The loss of chemisorbed oxygen may play a role in lowering the WF of ITO surface under UV illumination [45, 46].

In the case of ZnO, the surface C 1s spectrum was essentially identical for the pristine and the UV –exposed samples (Figure S3.c). The surface O 1s core level spectrum (Figure 6(I).a) of the pristine film included contributions from oxygen on lattice sites (O_l) with a peak at 531.6 eV and oxygen in vacancy sites or defects (O_v) at 533.2 eV. Exposure to UV does not alter the binding energy of these bands. The Zn 2p spectra (Figure 6(II).a) showed bands at 1023.1 eV and 1046.2 eV, typical of crystalline ZnO [48i], and were again essentially the same in the pristine and the UV exposed samples. XPS spectra collected after sputtering the EEL, and hence from a region closer to the ITO/EEL interface, show essentially the same bands for all C 1s, O 1s and Zn 2p electrons (Figures S3.d, 6(I).b and 6(II).b, respectively) but with a small shift, amounting to about 0.2-0.6eV, in both the pristine and the UV exposed samples. Additionally, the relative intensities of O_l and O_v were different, giving a O_l/O_v intensity ratio of ~ 2.7 instead of 0.3 in case of the surface spectra of the pristine samples. The lower ratio at the surface suggests that more defects and vacancy sites are present closer to the ZnO surface.

Turning now to the case of ZnO:PEI, the surface C 1s spectrum was again essentially identical for the pristine and the UV–exposed samples (Figure S3.e). The surface O 1s core level spectrum (Figure 6(I).c) of the pristine film again included contributions from O_l and O_v, with peaks at 531.4 eV and 533

eV, respectively, plus, a third component with a peak at 534.6 eV associated with chemisorbed molecules and/or hydroxyl groups (O_c). The O_l and O_v bands were not altered by the UV exposure and only the chemisorbed oxygen band, O_c showed a 0.5 eV increase in binding energy. The Zn 2p spectra (Figure 6(II).c) showed bands at 1022.8 eV and 1045.9 eV, typical of crystalline ZnO [48] and were again essentially the same in the pristine and the UV exposed samples. In general, a comparison of all C 1s, O 1s, and Zn 2p bands with those of the ZnO EEL discussed previously shows a ~0.2-0.3 eV shift to lower binding energies. A rigid shift in all bands suggests that it may be due to a dipole formation, perhaps arising from the presence of the PEI which contains amine groups. Interestingly, and in marked contrast to the surface spectra and to results from the ITO/ZnO sample, XPS spectra collected after sputtering the ZnO:PEI, and thus from a region closer to the ITO/EEL interface, show new bands in the UV exposed samples. The O 1s spectrum of the UV-exposed sample (Figure 6(I).d) shows new bands at 535.3 eV and 537.6 eV which are characteristic of O in zinc acetate and carbonyl groups [48, 49], respectively. Similarly, the Zn 2p spectrum of the UV-exposed sample (Figure 6(II).d) shows new bands at 1026.1 eV and 1049.2 eV which are usually assigned to Zn-C bonds in zinc acetate. The appearance of these new bands points to the formation of new chemical species from reactions activated by the UV excitation. That these bands exist more near the ITO interface and only in case of the ITO/ZnO:PEI sample indicates that species from both PEI and ITO are involved in those reactions. The results therefore indicate the formation of a new “chemical interface” in case of the ITO/ZnO:PEI contact, under UV. The fact that this new “chemical interface” is created by UV and that the same contact, i.e. ITO/ZnO:PEI, gives the most stable surface potential, as evident from the KPFM measurements, suggests that the two phenomena may be correlated; i.e. that this new interface allows maintaining a more stable contact potential despite the UV exposure. Knowing that reactions between oxygen and ITO surface can occur under UV illumination and cause shifts in work function [43, 45], forming a chemical interface where a larger fraction of oxygen atoms are chemically bonded to other species can be expected to reduce such effects.

In addition to the abovementioned observations, comparing the C 1s, O 1s and Zn 2p electrons binding energy of the ZnO:PEI sample (Figures S3.f 6(I).d, and 6(II).d) with that of the ZnO sample near the ITO interface (Figures S3.d, 6(I).b, and 6(II).b, respectively), a larger shift to lower binding energy, amounting to about 0.4-0.9eV in case of ZnO:PEI, versus only 0.2-0.6eV in case of ZnO, is observed. The shift suggests that it can be due to a stronger dipole formation near the ITO interface. This stronger dipole formation may perhaps be behind the lower CPD in case of the pristine ZnO:PEI when compared to the pristine ZnO film, provided in Figure 5 and contributes to the somewhat better initial PV properties of OSCs with ZnO:PEI (Table 1) in agreement with previous reports [30].

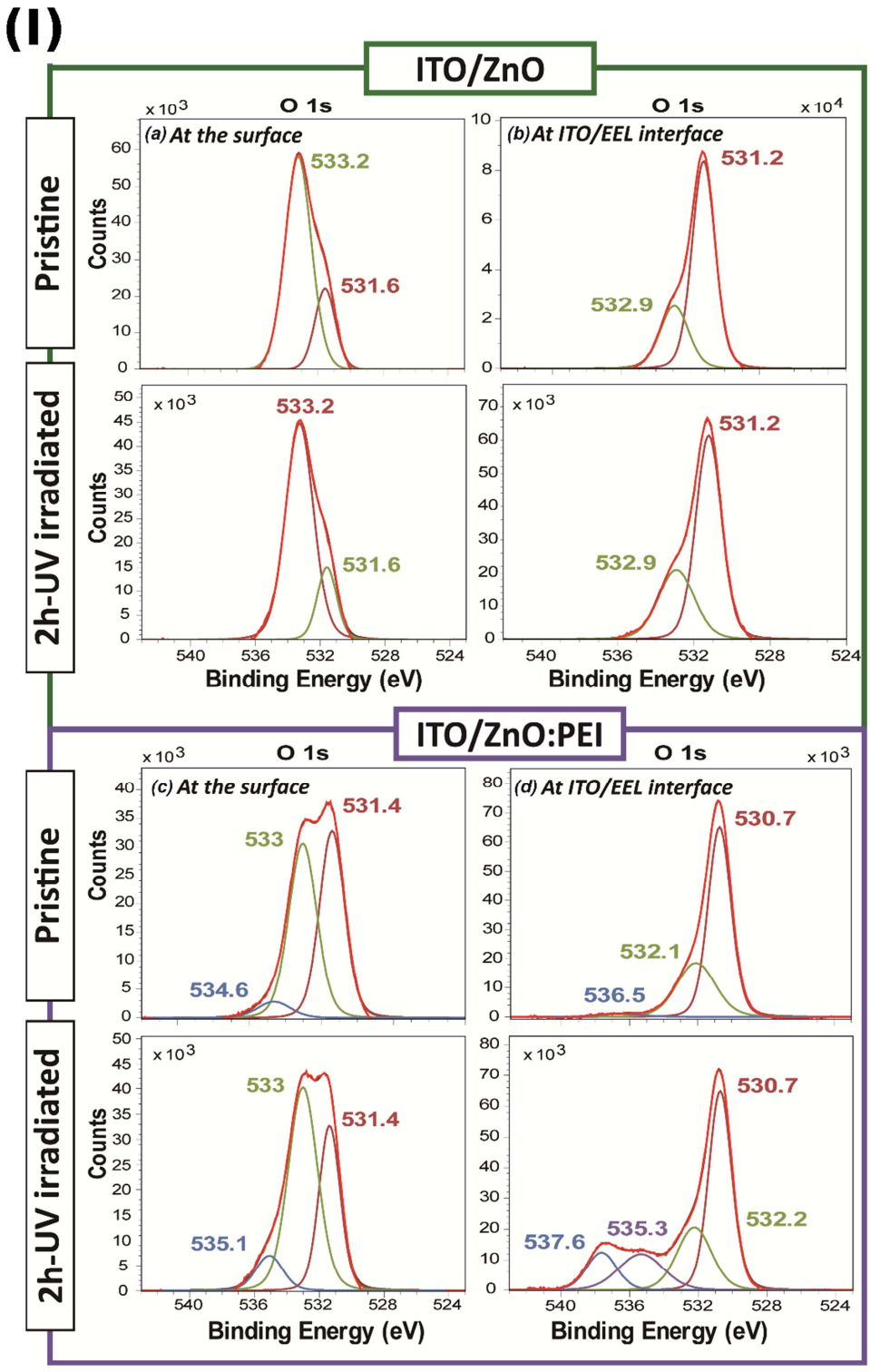
(I)
ITO/ZnO
Pristine
2h-UV irradiated
O 1s
(a) At the surface
533.2
531.6
(b) At ITO/EEL interface
531.2
532.9
Counts
Binding Energy (eV)
ITO/ZnO:PEI
(c) At the surface
531.4
533
534.6
(d) At ITO/EEL interface
530.7
532.1
536.5
535.1
537.6
535.3
532.2

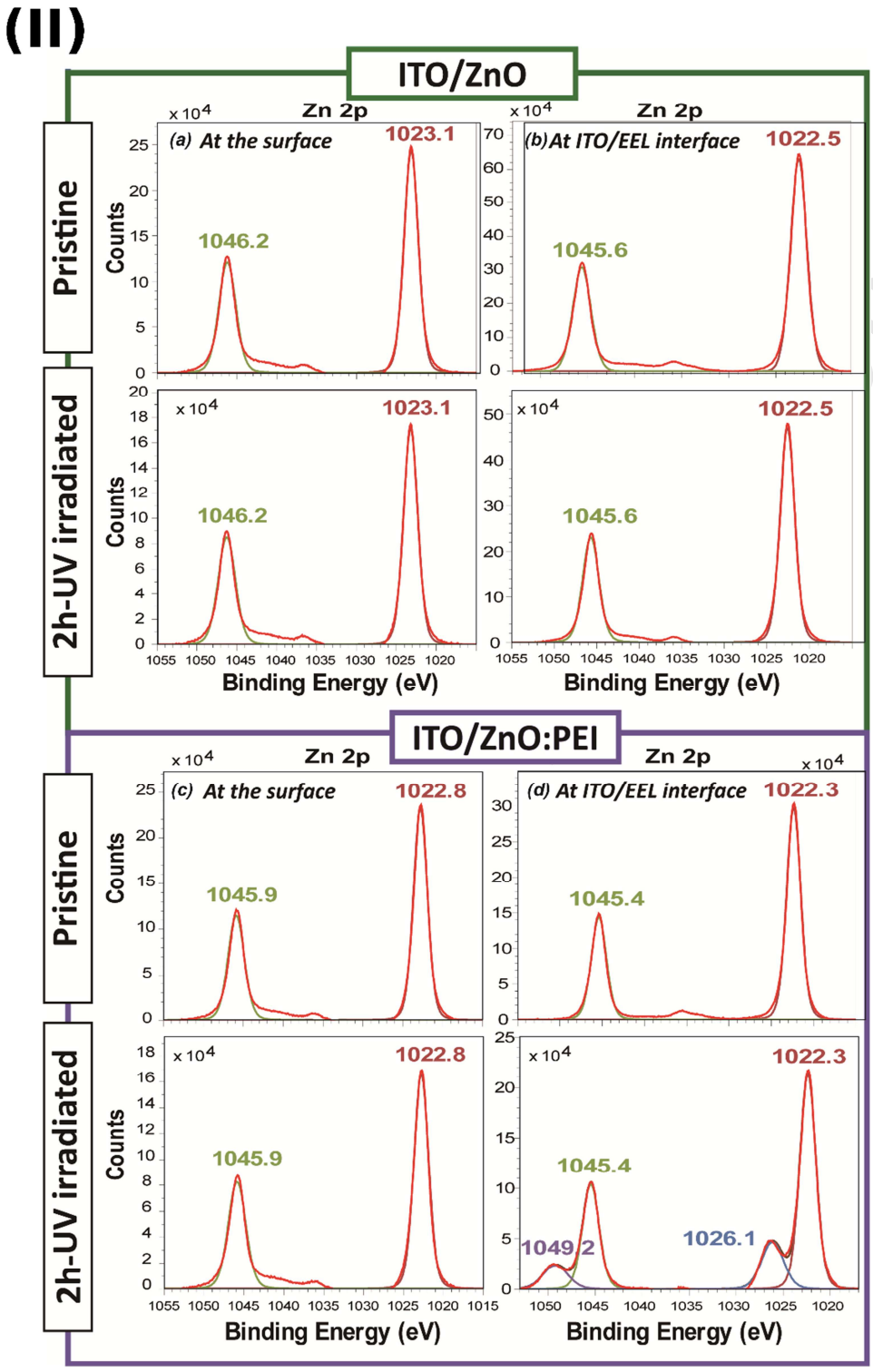

Figure 6. *XPS spectrum of (I). O 1s, and (II). Zn 2P, for pristine and UV irradiated ZnO and ZnO:PEI films; at the surface (a and c), and at the ITO/EEL interface (b and d).*

Based on the above results, a conclusion was made that the higher FF and V_{oc} photo-stability of the OSCs observed upon using the ZnO:PEI EEL was likely associated with chemical interactions between PEI and ITO at the ITO/ZnO:PEI interface that produced a more electronically and energetically stable contact that was less susceptible to changes in surface potential or work function by UV illumination. In order to further verify this conclusion, we test the effect of introducing a PEI layer in between the ITO and ZnO, i.e. using PEI/ZnO (bilayer), on OSC photo-stability performance. Should the above conclusions be correct, one would expect this new EEL configuration in which the PEI layer is in direct contact with ITO, to similarly lead to improved photo-stability. OSCs of the structure ITO/PEI/ZnO/P3HT:PC_{60}BM/MoO_3/Al are therefore made and tested, using the same procedures and conditions followed with the earlier set of OSCs. As before, the thickness of the PEI layer was about 5-7 nm, and the total thickness of the PEI/ZnO bilayer configuration was about 35-40 nms. The J_{sc}, V_{oc}, FF and PCE of this OSC were comparable to those of their counterparts with the ZnO/PEI (bilayer) EEL, and are provided in Table S2 for reference. Figure 7 presents the photo-stability test results under UV illumination, again showing changes in PV parameters over time, under UV exposure. Data from the earlier set of OSCs with a ZnO:PEI (mixture) EEL is also replotted for comparison. Clearly, the OSC with the PEI/ZnO (bilayer) EEL demonstrates the same enhanced photo-stability behaviour of the ZnO:PEI EEL OSC.

Results from devices with PEI/ZnO as an EEL prove that having PEI next to ITO indeed leads to maintaining more stable V_{oc} and FF in OSCs under UV exposure, ascertaining the previous conclusion that interactions between PEI and ITO lead to forming a stable electron collection contact. As the PCE of the PEI/ZnO device was lower than the other devices, using a ZnO:PEI EEL appears to be the most optimal approach for obtaining increased photo-stability.

In order to verify that the photo-stability enhancement upon using PEI in the ZnO EEL is not limited to P3HT:PC60BM-based OSCs, we also compare between the effect of using ZnO:PEI mixture and PEI/ZnO bilayer versus ZnO only as EELs in PCDTBT:PC70BM-based devices as an alternative BHJ material system. The device structure is ITO/EELs/PCDTBT:PC70BM/MoO_3/Al. Initial PV properties

are provided in Table S2. The results of the photo-stability test under UV illumination are shown in Figure 7. Clearly, once again, the OSCs with the ZnO:PEI mixture and PEI/ZnO bilayer EELs demonstrate a higher photo-stability compared to the ZnO EEL control. This clearly shows that the increased photo-stability is not specific to one D/A system.

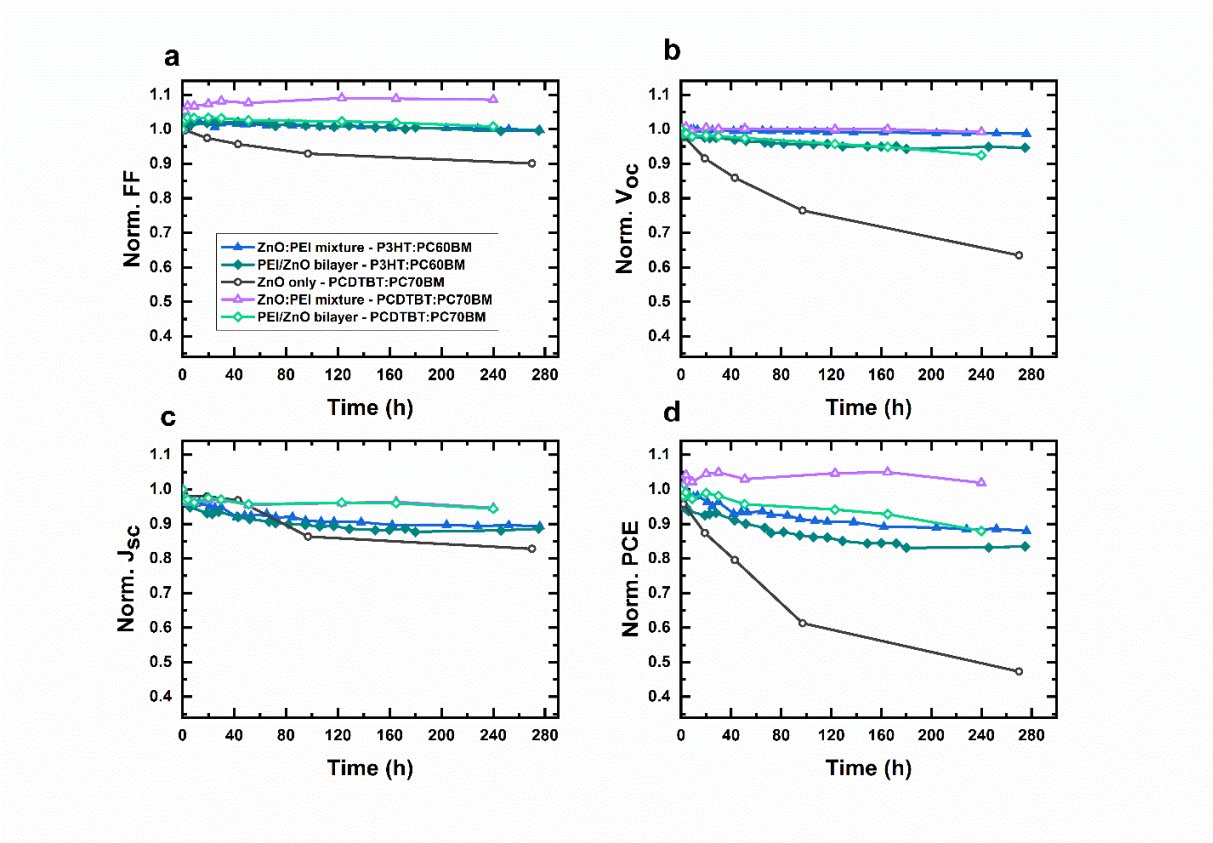

Figure 7. *Normalized FF (a), V_{oc} (b), J_{sc} (c), and PCE (d), versus time under continuous UV illumination of P3HT:PC60BM-based OSCs with the PEI/ZnO EEL, and PCDTBT:PC70BM-based OSCs with the ZnO, ZnO:PEI, and PEI/ZnO EELs. For the OSC with P3HT:PC60BM, data from the device with ZnO:PEI EEL is also included for comparison.*

4. Conclusions

In conclusion, results show that introducing PEI in the commonly used ZnO EELs reduces the susceptibility of OSCs to photo-degradation with the ZnO:PEI mixture providing a 5x higher PCE stability under continuous UV irradiation, mainly due to a more stable V_{oc} and FF. Using a ZnO/PEI

bilayer as the EEL also improves the photo-stability compared to the ZnO-based cells, suggesting that having PEI at the BHJ interface may have some photo-stability benefits. However, more significant stability enhancements of the ZnO:PEI mixture, as well as tests on electron only devices, show that the higher photo-stability of the ZnO:PEI mixture is mainly due to maintaining a more stable electron collection efficiency across the EEL and/or ITO/EEL contact. KPFM and XPS measurements reveal that the stability enhancement is associated with chemical interactions between PEI and ITO at the ITO/ZnO:PEI interface that produce a more electronically and energetically stable contact that is less susceptible to changes in surface potential or work function by UV illumination. Introducing a neat PEI layer in between the ITO and ZnO in the EEL (PEI/ZnO) similarly provides a significant photo-stability enhancement, ascertaining the above conclusions. The results not only reveal the potential of utilizing PEI in the EEL as an effective route to enhance OSC photo-stability, but also address some of the origins of the limited photo-stability of OSCs.

Conflicts of Interest

There are no conflicts of interest to declare.

Acknowledgements

The support by the Natural Sciences and Engineering Research Council of Canada (NSERC) and Canadian General Towers (CGT) Corporation is gratefully acknowledged.

Appendix A. Supporting Information

References

(1) Krebs, F. C. Fabrication and processing of polymer solar cells: a review of printing and coating techniques. Solar energy materials and solar cells 2009, 93 (4), 394-412.

(2) Li, G.; Zhu, R.; Yang, Y. Polymer solar cells. Nature photonics 2012, 6 (3), 153.

(3) Venkatesan, S.; Chen, Q.; Ngo, E. C.; Adhikari, N.; Nelson, K.; Dubey, A.; Sun, J.; Bommisetty, V.; Zhang, C.; Galipeau, D. Polymer solar cells processed using anisole as a relatively nontoxic solvent. Energy Technology 2014, 2 (3), 269-274.

(4) Aernouts, T.; Aleksandrov, T.; Girotto, C.; Genoe, J.; Poortmans, J. Polymer based organic solar cells using ink-jet printed active layers. Applied Physics Letters 2008, 92 (3), 22.

(5) Ngo, E.; Venkatesan, S.; Qiao, Q. Polymer photovoltaics with top metal electrode deposited by solution-processing. IEEE Transactions on Electron Devices 2014, 61 (8), 2957-2962.

(6) Venkatesan, S.; Ngo, E.; Khatiwada, D.; Zhang, C.; Qiao, Q. Enhanced lifetime of polymer solar cells by surface passivation of metal oxide buffer layers. ACS applied materials & interfaces 2015, 7 (29), 16093-16100.

(7) Sapkota, S. B.; Fischer, M.; Zimmermann, B.; Würfel, U. Analysis of the degradation mechanism of ITO-free organic solar cells under UV radiation. Solar Energy Materials and Solar Cells 2014, 121, 43-48.

(8) Jeong, J.; Seo, J.; Nam, S.; Han, H.; Kim, H.; Anthopoulos, T. D.; Bradley, D. D.; Kim, Y. Significant Stability Enhancement in High-Efficiency Polymer: Fullerene Bulk Heterojunction Solar Cells by Blocking Ultraviolet Photons from Solar Light. Advanced Science 2016, 3 (4), 1500269.

(9) Leijtens, T.; Eperon, G. E.; Pathak, S.; Abate, A.; Lee, M. M.; Snaith, H. J. Overcoming ultraviolet light instability of sensitized TiO 2 with meso-superstructured organometal tri-halide perovskite solar cells. Nature communications 2013, 4, 2885.

(10) Williams, G.; Aziz, H. The effect of charge extraction layers on the photo-stability of vacuum-deposited versus solution-coated organic solar cells. Organic Electronics 2014, 15 (1), 47-56.

(11) Williams, G.; Aziz, H. In Insights into electron and hole extraction layers for upright and inverted vacuum-deposited small molecule organic solar cells, Organic Photovoltaics XIV, International Society for Optics and Photonics: 2013; p 88301V.

(12) Williams, G.; Wang, Q.; Aziz, H. The photo-stability of polymer solar cells: Contact photo-degradation and the benefits of interfacial layers. Advanced Functional Materials 2013, 23 (18), 2239-2247.

(13) Wang, Q.; Williams, G.; Tsui, T.; Aziz, H. Photochemical deterioration of the organic/metal contacts in organic optoelectronic devices. Journal of Applied Physics 2012, 112 (6), 064502.

(14) MacLeod, B. A.; de Villers, B. J. T.; Schulz, P.; Ndione, P. F.; Kim, H.; Giordano, A. J.; Zhu, K.; Marder, S. R.; Graham, S.; Berry, J. J. Stability of inverted organic solar cells with ZnO contact layers deposited from precursor solutions. Energy & Environmental Science 2015, 8 (2), 592-601.

(15) Liang, Z.; Zhang, Q.; Wiranwetchayan, O.; Xi, J.; Yang, Z.; Park, K.; Li, C.; Cao, G. Effects of the morphology of a ZnO buffer layer on the photovoltaic performance of inverted polymer solar cells. Advanced Functional Materials 2012, 22 (10), 2194-2201.

(16) Hau, S. K.; Yip, H.-L.; Baek, N. S.; Zou, J.; O'Malley, K.; Jen, A. K.-Y. Air-stable inverted flexible polymer solar cells using zinc oxide nanoparticles as an electron selective layer. Applied Physics Letters 2008, 92 (25), 225.

(17) Liu, Q.; Toudert, J.; Liu, F.; Mantilla-Perez, P.; Bajo, M. M.; Russell, T. P.; Martorell, J. Circumventing UV Light Induced Nanomorphology Disorder to Achieve Long Lifetime PTB7-Th: PCBM Based Solar Cells. Advanced Energy Materials 2017, 7 (21), 1701201.

(18) Sun, Y.; Seo, J. H.; Takacs, C. J.; Seifter, J.; Heeger, A. J. Inverted polymer solar cells integrated with a low-temperature-annealed sol-gel-derived ZnO film as an electron transport layer. Advanced Materials 2011, 23 (14), 1679-1683.

(19) Ma, Z.; Tang, Z.; Wang, E.; Andersson, M. R.; Inganäs, O.; Zhang, F. Influences of surface roughness of ZnO electron transport layer on the photovoltaic performance of organic inverted solar cells. The Journal of Physical Chemistry C 2012, 116 (46), 24462-24468.

(20) Small, C. E.; Chen, S.; Subbiah, J.; Amb, C. M.; Tsang, S.-W.; Lai, T.-H.; Reynolds, J. R.; So, F. High-efficiency inverted dithienogermole–thienopyrrolodione-based polymer solar cells. Nature Photonics 2012, 6 (2), 115.

(21) Hau, S. K.; Yip, H.-L.; Jen, A. K.-Y. A review on the development of the inverted polymer solar cell architecture. Polymer Reviews 2010, 50 (4), 474-510.

(22) Yang, T.; Wang, M.; Duan, C.; Hu, X.; Huang, L.; Peng, J.; Huang, F.; Gong, X. Inverted polymer solar cells with 8.4% efficiency by conjugated polyelectrolyte. Energy & Environmental Science 2012, 5 (8), 8208-8214.

(23) Courtright, B. A.; Jenekhe, S. A. Polyethylenimine interfacial layers in inverted organic photovoltaic devices: Effects of ethoxylation and molecular weight on efficiency and temporal stability. ACS applied materials & interfaces 2015, 7 (47), 26167-26175.

(24) Woo, S.; Hyun Kim, W.; Kim, H.; Yi, Y.; Lyu, H. K.; Kim, Y. 8.9% Single-Stack Inverted Polymer Solar Cells with Electron-Rich Polymer Nanolayer-Modified Inorganic Electron-Collecting Buffer Layers. Advanced Energy Materials 2014, 4 (7), 1301692.

(25) Wang, C.; Mueller, C. J.; Gann, E.; Liu, A. C.; Thelakkat, M.; McNeill, C. R. Influence of fluorination on the microstructure and performance of diketopyrrolopyrrole-based polymer solar cells. Journal of Polymer Science Part B: Polymer Physics 2017, 55 (1), 49-59.

(26) Ye, P.; Chen, Y.; Wu, J.; Wu, X.; Yu, S.; Xing, W.; Liu, Q.; Jia, X.; Peng, A.; Huang, H. Wide bandgap small molecular acceptors for low energy loss organic solar cells. Journal of Materials Chemistry C 2017, 5 (47), 12591-12596.

(27) Park, M.; Jung, J. W. Anthracene-based perylene diimide electron-acceptor for fullerene-free organic solar cells. Dyes and Pigments 2017, 143, 301-307.

(28) Jia, X.; Wu, N.; Wei, J.; Zhang, L.; Luo, Q.; Bao, Z.; Li, Y.-Q.; Yang, Y.; Liu, X.; Ma, C.-Q. A low-cost and low-temperature processable zinc oxide-polyethylenimine (ZnO: PEI) nano-composite as cathode buffer layer for organic and perovskite solar cells. Organic Electronics 2016, 38, 150-157.

(29) Chen, H.-C.; Lin, S.-W.; Jiang, J.-M.; Su, Y.-W.; Wei, K.-H. Solution-processed zinc oxide/polyethylenimine nanocomposites as tunable electron transport layers for highly efficient bulk heterojunction polymer solar cells. ACS applied materials & interfaces 2015, 7 (11), 6273-6281.

(30) Liu, C.; Li, Z.; Zhang, X.; Guo, W.; Zhang, L.; Ruan, S. Annealing-Free ZnO: PEI Composite Cathode Interfacial Layer for Efficient Organic Solar Cells. ACS Photonics 2017, 4 (11), 2952-2958.

(31) Rasool, S.; Van Doan, V.; Lee, H. K.; Lee, S. K.; Lee, J. C.; Moon, S. J.; ... & Shin, W. S. Enhanced photostability in polymer solar cells achieved with modified electron transport layer. Thin Solid Films 2019, 669, 42-48.

(32) Tournebize, A. l.; Mattana, G.; Gorisse, T. r. s.; Bousquet, A.; Wantz, G.; Hirsch, L.; Chambon, S. Crucial Role of the Electron Transport Layer and UV Light on the Open-Circuit Voltage Loss in Inverted Organic Solar Cells. ACS applied materials & interfaces 2017, 9 (39), 34131-34138.

(33) Davidson-Hall, T.; Aziz, H. The role of polyethylenimine in enhancing the efficiency of quantum dot light-emitting devices. Nanoscale 2018, 10 (5), 2623-2631.

(34) Prosa, M.; Tessarolo, M.; Bolognesi, M.; Margeat, O.; Gedefaw, D.; Gaceur, M.; Videlot-Ackermann, C.; Andersson, M. R.; Muccini, M.; Seri, M. Enhanced ultraviolet stability of air-processed polymer solar cells by Al doping of the ZnO interlayer. ACS applied materials & interfaces 2016, 8 (3), 1635-1643.

(35) Kam, Z.; Wang, X.; Zhang, J.; Wu, J. Elimination of burn-in open-circuit voltage degradation by ZnO surface modification in organic solar cells. ACS applied materials & interfaces 2015, 7 (3), 1608-1615.

(36) Heumueller, T.; Mateker, W. R.; Distler, A.; Fritze, U. F.; Cheacharoen, R.; Nguyen, W. H.; Biele, M.; Salvador, M.; von Delius, M.; Egelhaaf, H.-J. Morphological and electrical control of fullerene

dimerization determines organic photovoltaic stability. Energy & Environmental Science 2016, 9 (1), 247-256.

(37) Wu, C. C.; Lin, Y. T.; Wong, K. T.; Chen, R. T.; Chien, Y. Y. Efficient Organic Blue-Light-Emitting Devices with Double Confinement on Terfluorenes with Ambipolar Carrier Transport Properties. Advanced Materials 2004, 16 (1), 61-65.

(38) Trost, S.; Zilberberg, K.; Behrendt, A.; Polywka, A.; Görrn, P.; Reckers, P.; Maibach, J.; Mayer, T.; Riedl, T. Overcoming the "Light-Soaking" Issue in Inverted Organic Solar Cells by the Use of Al: ZnO Electron Extraction Layers. Advanced Energy Materials 2013, 3 (11), 1437-1444.

(39) Cho, Y. J.; Aziz, H. The Root Causes of the Limited Electroluminescence Stability of Organic Light-emitting Devices Made by Solution-coating. ACS applied materials & interfaces 2018.

(40) Wang, Q.; Sun, B.; Aziz, H. Exciton–Polaron-Induced Aggregation of Wide-Bandgap Materials and its Implication on the Electroluminescence Stability of Phosphorescent Organic Light-Emitting Devices. Advanced Functional Materials 2014, 24 (20), 2975-2985.

(41) Manor, A.; Katz, E. A.; Tromholt, T.; Krebs, F. C. Electrical and Photo-Induced Degradation of ZnO Layers in Organic Photovoltaics. Advanced Energy Materials 2011, 1 (5), 836-843.

(42) Manor, A.; Katz, E.A.; Tromholt, T.; Krebs, F.C. Enhancing functionality of ZnO hole blocking layer in organic photovoltaics. Solar Energy Materials and Solar Cells 2012, 98, 491-493.

(43) Olivier, J.; Servet, B.; Vergnolle, M.; Mosca, M.; Garry, G. Stability/instability of conductivity and work function changes of ITO thin films, UV-irradiated in air or vacuum: Measurements by the four-probe method and by Kelvin force microscopy. Synthetic Metals 2001, 122 (1), 87-89.

(44) Trost, S.; Becker, T.; Polywka, A.; Görrn, P.; Oszajca, M. F.; Luechinger, N. A.; Rogalla, D.; Weidner, M.; Reckers, P.; Mayer, T. Avoiding photoinduced shunts in organic solar cells by the use of tin oxide (SnOx) as electron extraction material instead of ZnO. Advanced Energy Materials 2016, 6 (15), 1600347.

(45) Girtan, M.; Rusu, M. Role of ITO and PEDOT: PSS in stability/degradation of polymer: fullerene bulk heterojunctions solar cells. Solar Energy Materials and Solar Cells 2010, 94 (3), 446-450.

(46) Zhou, Y.; Shim, J. W.; Fuentes-Hernandez, C.; Sharma, A.; Knauer, K. A.; Giordano, A. J.; Marder, S. R.; Kippelen, B. Direct correlation between work function of indium-tin-oxide electrodes and solar cell performance influenced by ultraviolet irradiation and air exposure. Physical Chemistry Chemical Physics 2012, 14 (34), 12014-12021.

(47) Turak, A. Interfacial degradation in organic optoelectronics. RSC Advances 2013, 3(18), 6188-6225.

(48) Mar, L. G.; Timbrell, P. Y.; Lamb, R. N. An XPS study of zinc oxide thin film growth on copper using zinc acetate as a precursor. Thin Solid Films 1993, 223 (2), 341-347.

(49) Tillborg, H.; Nilsson, A.; Hernnäs, B.; Mårtensson, N.; Palmer, R. X-ray and UV photoemission studies of mono-, bi-and multilayers of physisorbed molecules: O2 and N2 on graphite. Surface science 1993, 295 (1-2), 1-12.

Appendix A. Supporting Information

Enhanced Photo-stability of Inverted Organic Solar Cells via Using Polyethylenimine in the Electron Extraction Layers

Mozhgan Sadeghianlemraski[4] 2, Brenda Yasie Lee[5 6], Tyler Davidson-Hall[1 2], Zoya Leonenko2 3, Hany Aziz1 2

[4] Department of Electrical and Computer Engineering, University of Waterloo, 200 University Avenue West, Waterloo, ON N2L 3G1, Canada.

[5] Waterloo Institute of Nanotechnology, University of Waterloo, 200 University Avenue West, Waterloo, ON N2L 3G1, Canada.

[6] Department of Physics & Astronomy, University of Waterloo, 200 University Avenue West, Waterloo, ON N2L 3G1, Canada.

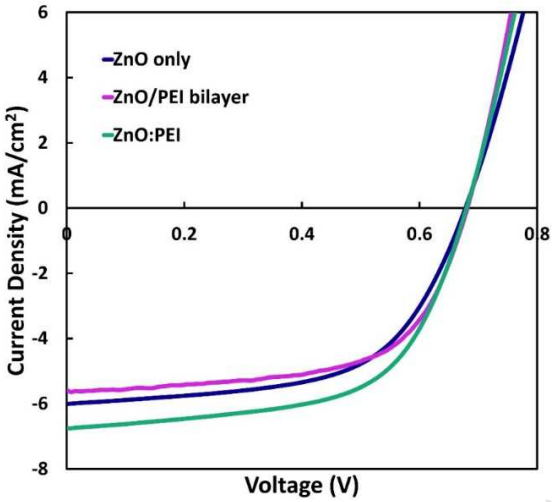

Figure S1. *JV characteristics of OSCs with the highest PCE with the ZnO, ZnO/PEI and ZnO:PEI EELs, measured under 1-sun AM1.5G illumination.*

Table S1. *PV parameters of OSCs with ZnO:PEI EEL with different weight mixing ratios of (1:0.01), (1:0.02), (1:0.03), and (1:0.04).*

ZnO:PEI %wt / ***Parameters***	***1 : 0.01***	***1: 0.02***	***1: 0.03***	***1: 0.04***
$J_{sc}(mA/cm^2)$	6.18	6.31	6.14	6.75
$V_{oc}\ (mV)$	676	672	685	679
FF [%]	56.04	55.68	58.68	59.97
$R_{shunt}\ (Ohm.\ cm^2)$	19168	16200	26727	18731
R_{series} $(Ohm.\ cm^2)$	13.76	9.59	13.91	8.57
PCE [%]	2.34	2.36	2.46	2.75

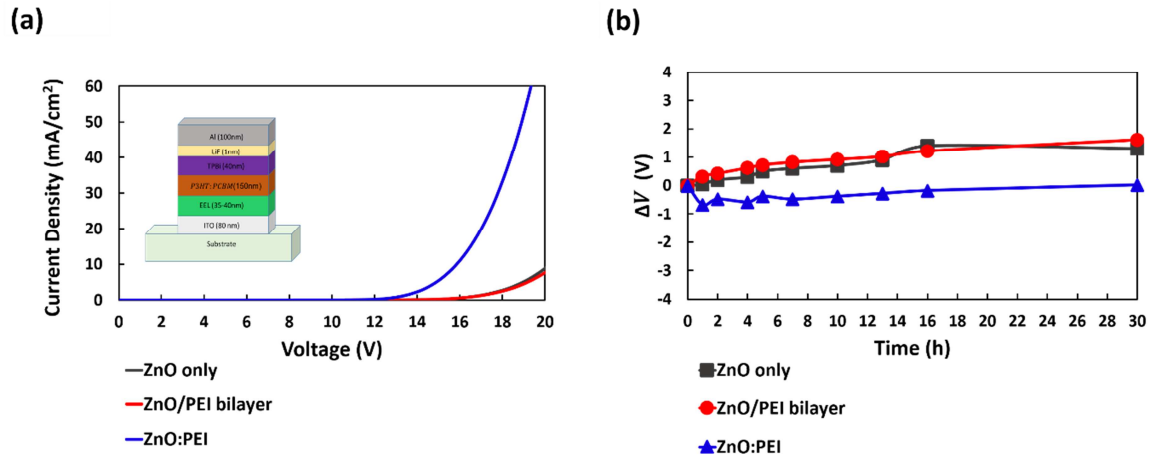

Figure S2. *a) JV characteristics collected in the dark for EODs with ZnO, ZnO/PEI or ZnO:PEI contacts. Insets: the structure of EODs used in this part. b) Net change in driving voltage (ΔV) defined as voltage needed to maintain a current density of 20 mA/cm² at any time t minus the initial voltage at the same current density, under 5h UV illumination for the 3 contacts of interests.*

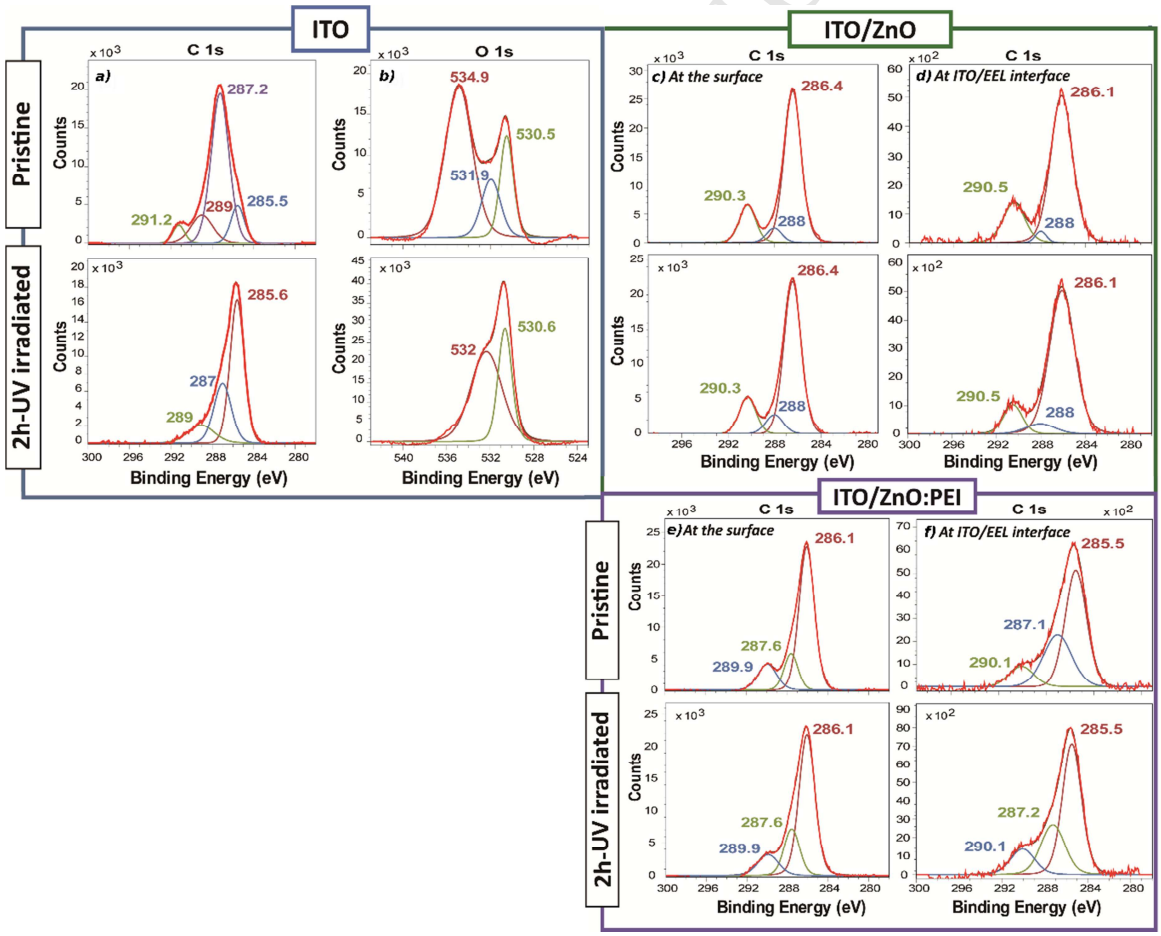

Figure S3. *C 1s and O 1s peaks of pristine and 2h-UV-irradiated ITO (left), and C 1s peaks of pristine and 2h-UV-irradiated ITO/ZnO and ITO/ZnO:PEI (right), at the surface versus at the ITO/EEL interface.*

Table S2. *PV parameters of P3HT:PC60BM-based OSCs with the PEI/ZnO bilayer EEL, and PCDTBT:PC70BM-based OSCs with the ZnO, ZnO:PEI, and PEI/ZnO EELs.*

Parameters / ***Device***	J_{sc} (mA/cm^2)	V_{oc} (mV)	FF [%]	R_{shunt} $(Ohm.cm^2)$	R_{series} $(Ohm.cm^2)$	PCE [%]
PEI/ZnO – P3HT:PC60BM	6.39	660.32	55.30	21229	15.40	2.33
ZnO – PCDTBT:PC70BM	10.12	822.12	51.41	14706	10.275	4.28
ZnO:PEI – PCDTBT:PC70BM	10.67	872.97	47.31	11479	10.635	4.41
PEI/ZnO – PCDTBT:PC70BM	10.23	869.46	48.58	13547	11.332	4.32

Highlights

- Introducing PEI in the commonly used ZnO EELs, either as a mixture (ZnO:PEI) or a bilayer (ZnO/PEI), reduces the susceptibility of OSCs to photo-degradation with the mixture giving more significant stability enhancements.

- The use of ZnO:PEI mixture leads to ~ 5x higher PCE stability under continuous illumination, compared to the commonly used ZnO, primarily due to a more stable V_{oc} and FF.

- The ITO/EEL interface plays a critical role in the photo-stability of OSCs.

- The higher photo-stability of ZnO:PEI-based OSCs is originated from chemical interactions between PEI and ITO at the ITO/ZnO:PEI interface that produce a more electronically and energetically stable contact.